Schwertmannite, a new iron oxyhydroxysulphate from Pyhäsalmi, Finland, and other localities

J. M. BIGHAM

School of Natural Resources, The Ohio State University, 2021 Coffey Road, Columbus, Ohio, 43210-1086, U.S.A.

L. CARLSON

Pietarinkatu 10 B 16, FIN-00140 Helsinki, Finland

AND

E. MURAD*

Lehrstuhl für Bodenkunde, Technische Universität München, D-85350 Freising-Weihenstephan, Germany

Abstract

Schwertmannite is a new oxyhydroxysulphate of iron from the Pyhäsalmi sulphide mine, Province of Oulu, Finland. It occurs there, and elsewhere, as an ochreous precipitate from acid, sulphate-rich waters. Associated minerals at other localities may include jarosite, natrojarosite, goethite and ferrihydrite. Schwertmannite is a poorly crystalline, yellowish brown mineral with a fibrous morphology under the electron microscope. A high specific surface area in the range of 100 to 200 m^2/g, rapid dissolution in cold, 5 M HCl or in ammonium oxalate at pH 3, and pronounced X-ray diffraction line broadening are consistent with its poorly crystalline character.

Colour parameters for the type specimen as related to CIE illuminant C are $L^* = 53.85$, $a^* = +15.93$, and $b^* = +47.96$. Chemical analysis gives Fe_2O_3, 62.6; SO_3, 12.7; CO_2, 1.5; H_2O^-, 10.2; H_2O^+, 12.9; total 99.9 wt.%. These data yield an empirical unit cell formula of $Fe_{16}O_{16}(OH)_{9.6}(SO_4)_{3.2}\cdot10H_2O$ after exclusion of CO_2 and H_2O^-. The most general simplified formula is $Fe_{16}O_{16}(OH)_y(SO_4)_z\cdot nH_2O$, where $16 - y = 2z$ and $2.0 \leqslant z \leqslant 3.5$. Schwertmannite has a structure akin to that of akaganéite (nominally β-FeOOH) with a doubled c dimension. Its X-ray powder diffraction pattern consists of eight broad peaks [d_{obs} in Å(I_{obs}) (hkl)] 4.86(37)(200,111); 3.39(46)(310); 2.55(100)(212); 2.28(23)(302); 1.95(12)(412); 1.66(21)(522); 1.51(24)(004); and 1.46(18)(204,542), giving $a = 10.66(4)$, $c = 6.04(1)$ Å, and $V = 686(6)$ Å^3 for a primitive, tetragonal unit cell. The probable space group is $P4/m$. Upon heating, schwertmannite transforms to hematite with $Fe_2(SO_4)_3$ occurring as an intermediate phase. Bidentate bridging complexes between Fe and SO_4 are apparent in infrared spectra. Mössbauer data show the Fe in schwertmannite to be exclusively trivalent and in octahedral coordination; it has a Néel temperature of 75 ± 5 K and a saturation magnetic hyperfine field of about 45.6 T. Pronounced asymmetry of the Mössbauer spectra indicates different locations for Fe atoms relative to SO_4 groups in the structure. The name is for Udo Schwertmann, professor of soil science at the Technical University of Munich.

KEYWORDS: schwertmannite, new mineral, acid mine drainage, iron, Pyhäsalmi, Finland

*Present address: Bayerisches Geologisches Landesamt, Staatliches Forschungsinstitut für Geochemie, Concordiastraße 28, D-96049 Bamberg, Germany.

Introduction

SCHWERTMANNITE, a newly recognized oxyhydroxy-sulphate of iron, was first encountered during the characterization of ochreous precipitates collected from acid coal mine drainage in Ohio, U.S.A. Additional samples were subsequently acquired from a variety of sources and locations (see later discussion). The type specimen of schwertmannite described in this paper is the purest sample discovered to date. The new species has been named in honor of Udo Schwertmann (1927–), professor of soil science at the Technical University of Munich. Prof. Schwertmann has made numerous contributions to the crystal chemistry of iron oxides and oxyhydroxides and has greatly advanced our knowledge of poorly crystalline phases that are common to weathering environments. Both the mineral and its name were approved by the Commission on New Minerals and Mineral Names in 1992 (90-006). Type specimens (co-types) are now held in the collection of the Geological Museum at the University of Helsinki (a department of the Finnish Museum of Natural History) in Helsinki, Finland.

Occurrence

The reference specimen, identified as Py-4 and catalogued as B 8659 by the Finnish Museum of Natural History, was acquired from an ore processing area of the Pyhäsalmi sulphide mine (pyrite, sphalerite, chalcopyrite, pyrrhotite, galena, arsenopyrite), Province of Oulu, Finland (63°39.6'N, 26°02'E). The sample was collected as an ochreous, secondary precipitate forming a crust on stones inundated by acidic (pH 3.2) drainage from a mound of concentrate sand. The geochemical environment is typical of other known occurrences of schwertmannite. Specifically, the mineral usually forms as a result of the rapid oxidation of Fe^{2+} in acid, sulphate-rich effluents produced by the decomposition of primary sulphides (Bigham *et al.*, 1992). It is often the major component of what has previously been described as precipitates of 'amorphous' ferric hydroxide from acid mine drainage. A pH range of 3.0 to 4.5 and sulphate concentrations in the range of 1000 to 3000 mg/L are optimum for the formation of schwertmannite. At lower pHs, jarosite or natrojarosite may form as ancillary phases if $[SO_4^{2-}]$ is sufficiently high. Goethite is also a commonly associated phase and may be an alteration product of schwertmannite, especially at pHs exceeding 4.5.

Schwertmannite has been synthesized in the laboratory using both abiotic and biotic techni-ques. The former have involved the rapid hydrolysis of ferric nitrate/chloride solutions doped with sulphate (Brady *et al.*, 1986; Bigham *et al.*, 1990). The latter have been based upon the bacterial oxidation of acid, $FeSO_4$ solutions using strains of *Thiobacillus ferrooxidans* (Lazaroff *et al.*, 1982, 1985; Bigham *et al.*, 1990) in either batch or dynamic fermentation systems. In these cases, the oxidation reaction is bacterially mediated, but the mineralization process is extracellular so that mineral speciation is still controlled by geochemical parameters (pH, $[SO_4^{2-}]$, $[Fe^{3+}]$, etc.).

Physical properties

Schwertmannite is a poorly crystalline mineral with a high specific surface area, usually in the range of 100 to 200 m^2/g. Most specimens consist of spherical to ellipsoidal particles (aggregates) that are 200 to 500 nm in diameter (Fig. 1). Needle-like structures with average widths and thicknesses of 2 to 4 nm and lengths of 60 to 90 nm radiate from the particle surfaces to give a 'pin-cushion' morphology. Schwertmannite is brownish yellow in colour. Precise colour calculations using reflectance data collected from the type specimen with a tristimulus colourimeter are presented in Table 1 employing both CIE and Munsell notations. Other optical parameters could not be measured due to the extremely fine grain size of the mineral. True density determinations were also not possible because of the small crystal size; however, the calculated density, based on the unit-cell dimensions and simplified formulae given below, ranges from 3.77 to 3.99 g/cm^3.
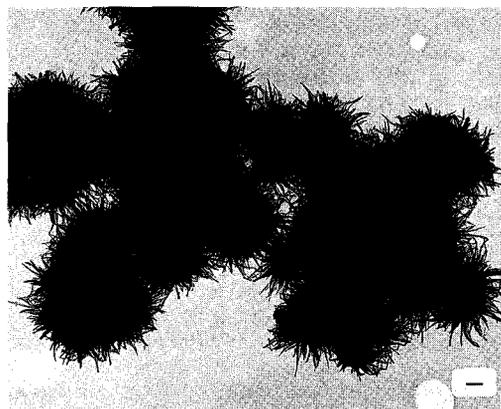

FIG. 1. Transmission electron micrograph of schwert-mannite. Scale bar = 0.1 μm.

TABLE 1. Colour parameters for schwertmannite (sample Py-4) relative to CIE illuminant C

	CIE[†]			Munsell		
L*	a*	b*		Hue	Value	Chroma
53.85	+15.93	+47.96		8.0YR	5.3	8.1

[†]Commission Internationale de l'Eclairage (1978).

Chemical composition

Schwertmannite has been found to be readily soluble (about 15 min) in cold, 5 M HCl or in pH 3.0, 0.2 M ammonium oxalate. Total Fe and S in the type specimen were determined after dissolution of the sample in ammonium oxalate followed by analysis with a Jobin Yvon 70+ inductively-coupled plasma emission spectrometer. Total S was also obtained by a combustion procedure using a Leco Model 521 induction furnace. In this procedure, SO_2 evolved at 1000°C was collected in a starch solution and quantified using a semiautomatic titrator with KIO_3 as the titrant. Total C was quantified using a Leybold-Heraeus Series 302 instrument wherein the evolution of CO_2 was monitored with an infrared analyser after combustion of the sample in an O_2 atmosphere at 1000°C. Weight losses after static heating to 100°C and 800°C for 24 h were also measured to obtain H_2O contents.

The results presented in Table 2 are from the type specimen (Py-4) and a synthetic sample (Z510b) of schwertmannite. The latter is described in more detail elsewhere (Bigham et al., 1990). The analyses yield empirical unit cell formulae of $Fe_{16}O_{16}(OH)_{9.6}(SO_4)_{3.2} \cdot 10H_2O$ for

TABLE 2. Chemical composition of schwertmannite

Constituent	Py-4 (wt.%)	Z 510b[†] (wt.%) (synthetic)
Fe_2O_3	62.6	61.8
SO_3	12.7	12.9
CO_2	1.5	0.2
H_2O^-	10.2	9.8
H_2O^+	12.9	14.1
Total	99.9	98.8
Fe/S	4.9	4.8

[†]Sample prepared by oxidation of a 4% $FeSO_4$ solution at pH 3.0

Py-4 and $Fe_{16}O_{16}(OH)_{9.4}(SO_4)_{3.3} \cdot 12H_2O$ for Z510b. These formulae were calculated by balancing the total anion charge against an ideal total cation charge of 48 arising entirely from Fe after the data were adjusted to exclude CO_2 and adsorbed water (H_2O^-). The Fe/O ratio was taken as 1 (as in the Fe oxyhydroxides) and all anionic substitution was assumed to occur at the expense of OH (see discussion under crystal structure for further explanation).

Powder X-ray diffraction

X-ray diffraction analyses of backfill powder mounts were conducted using Co-$K\alpha$ radiation with a Philips PW 1070 goniometer equipped with a diffracted-beam monochromator and a 1° divergence slit. The specimen was step scanned from 10 to 80° 2θ in increments of 0.05° 2θ with 20 s counting time and with silicon as an internal standard. The digitized scan was then fitted with the FIT curve program of Janik and Raupach (1977) as modified by H. Stanjek (unpubl. data). Unit-cell edge lengths were subsequently calculated with the program GITTER (W. Hummel, unpubl. data) using six tanθ weighted reflections.

The X-ray powder diffraction pattern of schwertmannite consists of eight broad diffraction bands (Fig. 2), resulting in rather low accuracy of measurement. Band intensities, d-values, and full widths at half maxima (FWHM) are presented in Table 3. The pattern was indexed based on a modified hollandite/akaganéite structure with a primitive tetragonal cell as described below. The resulting unit cell parameters, as refined from the powder data, are $a = 10.66(4)$Å, $c = 6.04(1)$Å, and $V = 686(6)$Å³ with $Z = 1$. The probable space group is $P4/m$.

Thermal properties

Simultaneous differential thermal and thermogravimetric analyses (DTA, TGA) were performed with a Linseis instrument operated at a heating rate of 10°C/min in air with 40 to 50 mg of dry
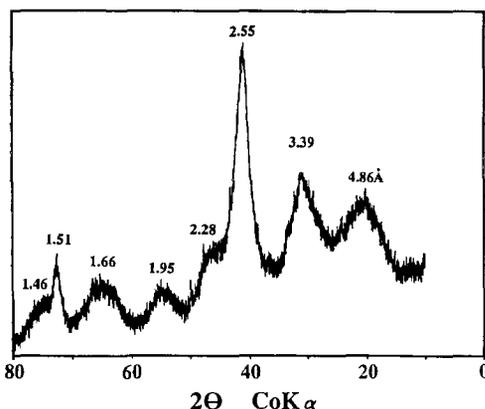
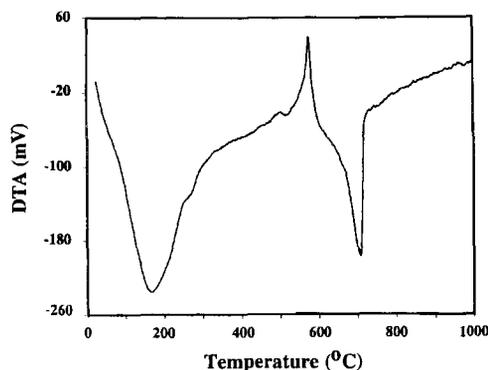FIG. 2. X-ray powder diffraction pattern of schwert-
mannite (sample Py-4).

FIG. 3. DTA pattern of schwertmannite (sample Py-4)
following treatment with H_2O_2 to remove organic
matter.

(over P_2O_5) sample and hematite as an inert
reference material.

The thermal decomposition of schwertmannite
produces a low-temperature endotherm between
100 and 300°C followed by an exotherm at 540 to
580°C that immediately gives way to a second
endothermic reaction in the range of 650 to 710°C
(Fig. 3). The initial endothermic reaction is
associated with a weight loss of 20 to 25% that
results from the vaporization of sorbed H_2O as
well as structural OH/H_2O. X-ray diffraction
analyses of samples taken after quenching of the
thermal reaction at various temperatures show
that hematite forms prior to onset of the

TABLE 3. X-ray powder date for schwertmannite
(sample Py-4)

I/I_o	d_{obs}(Å)	d_{calc}(Å)	*hkl*	FWHM (°2θ)
37	4.86	4.73	200 / 111 } comp.	7.0
46	3.39	3.37	310	5.4
100	2.55	2.56	212	3.2
23	2.28	2.31	302	4.7
12	1.95	1.97	412	3.4
21	1.66	1.66	522	5.8
24	1.51	1.52	004	1.5
18	1.46	1.46	204 / 542 } comp.	5.7

Note:The tetragonal cell parameters refined from the
above data are $a = b = 10.66(4)$Å, $c = 6.04(1)$Å,
and $V = 686(6)$Å^3.

exothermic reaction at 560°C and that products
immediately following the reaction include both
hematite and $Fe_2(SO_4)_3$. Crystallization of the
latter may be responsible for the observed
exothermic effect. The final endotherm at 700°C
can be attributed to decomposition of $Fe_2(SO_4)_3$
to yield additional hematite and SO_3. Release of
the latter produces a weight loss of 6 to 12%.

Infrared spectroscopy

Diffuse reflectance, Fourier transform infrared
spectra were collected from a 5-mg sample of
schwertmannite mixed with 195 mg of spectro-
scopic grade KBr. Spectra were recorded as an
average of 500 scans made at 1 cm^{-1} resolution
using a Mattson-Polaris instrument equipped with
a broad-band, mercury-cadmium-telluride
detector, a KCl beam-splitter, and a Harrick
Praying-Mantis diffuse reflectance cell.

The infrared spectrum of sample Py-4 is
dominated by a broad, OH-stretching band
centered at 3300 cm^{-1} (Fig. 4). Another
prominent absorption feature related to H_2O
deformation is expressed at 1634 cm^{-1}. Intense
bands at 1186, 1124, and 1038 cm^{-1} reflect a
strong splitting of the v_3 (SO_4) fundamental due to
the formation of a bidentate bridging complex
between SO_4 and Fe. This complex may result
from the replacement of OH groups by SO_4 at the
mineral surface through ligand exchange or by the
formation of linkages within the structure during
nucleation and subsequent growth of the crystal.
Related features due to the presence of structural
SO_4 include bands at 976 and 608 cm^{-1} that can be
assigned to v_1 (SO_4) and $v_4(SO_4)$, respectively.
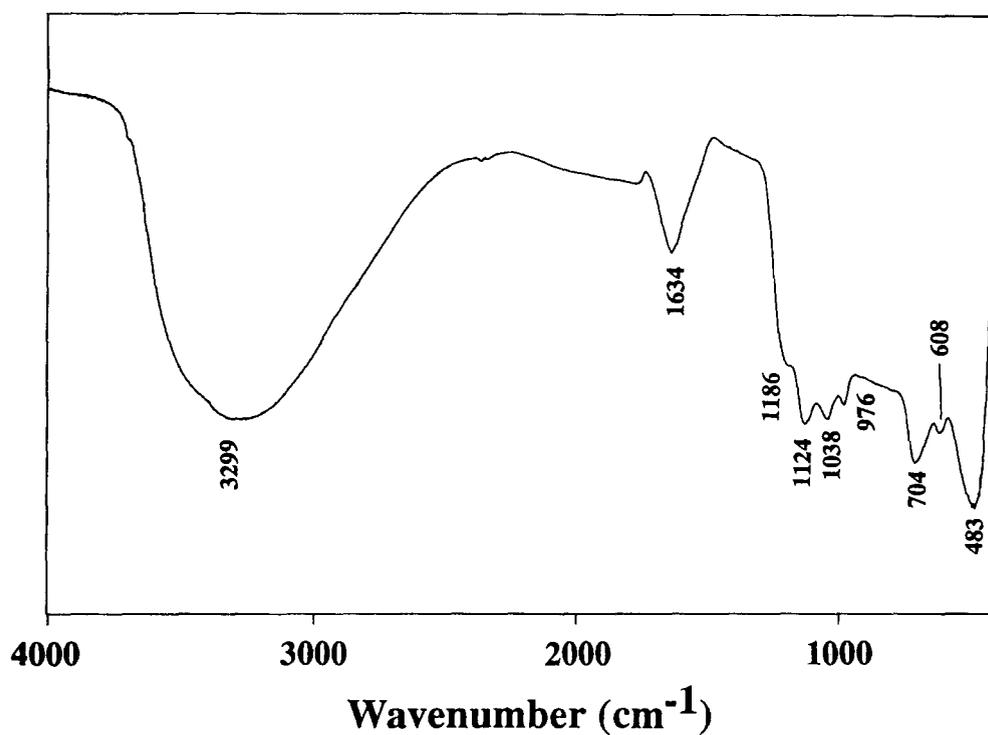Vibrations at 704 and 483 cm^{-1} are attributed to

FIG. 4. Infrared pattern of schwertmannite (sample Py-4).

Fe-O stretch; however, assignment of the former is tentative because similar bands in the iron oxyhydroxides usually occur at lower frequencies. A broad absorption shoulder in the 800 to 880 cm^{-1} range is apparent in some specimens and is related to OH deformation [δ(OH)].

Mössbauer spectroscopy

Mössbauer spectroscopy was conducted using a ^{57}Co/Rh source. Spectra were taken at room temperature, between 90 and 50 K, and at 4.2 K. Samples were mixed with two parts sugar and placed in plastic holders to produce absorbers containing between 10 and 12.5 mg schwertmannite per cm^2. The transmitted radiation was recorded with a proportional counter and stored in a 1024 channel analyser. A metallic iron foil was used for velocity calibration, and spectra were collected in the velocity ranges of ± 2 and ± 5 mm/s at room temperature and ± 10.5 mm/s at 4.2 K until sufficiently good statistics (between about 2.6×10^6 and 8×10^6 counts per channel) had been attained. The mirror halves of the spectra were folded and Lorentzian line fits carried out by a computer procedure constraining corresponding
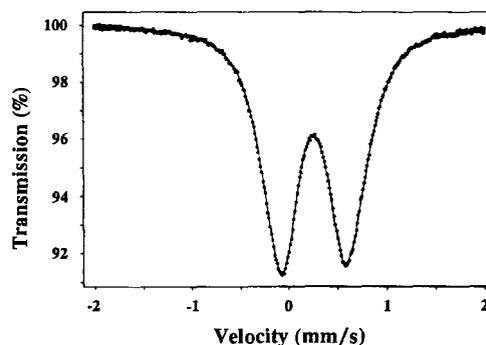

FIG. 5. Mössbauer spectrum of schwertmannite (sample Py-4) recorded at room temperature.

lines of every doublet and sextet to have equal widths and intensities. Spectra were plotted as measured (i.e. relative to the source), whereas isomer shifts were recalculated relative to the centroid of the room-temperature spectrum of metallic iron.

The room-temperature Mössbauer spectrum of schwertmannite consists of two broad, asymmetric lines. Of these, the low-velocity line has a higher

TABLE 4. Room-temperature Mössbauer parameters of schwertmannite (sample Py-4)

Fit	Δ_{max}[‡]	W_{dis}[‡]	δ/Fe	$\delta(\delta)$
VARISO[†]	0.64(1)	0.60	0.3578(6)	0.0038(2)
TWOISO[†]	0.64(1)	0.56	0.394 (3)	
	0.64(1)	0.59	0.341(3)	

[†] VARISO fits variable isomer shifts which increase from δ/Fe by $\delta(\delta)$ mm/s per 0.20 mm/s increment in quadrupole splitting; TWOISO fits two distributions of quadrupole splittings with discretely different isomer shifts.

[‡] Δ_{max} is the quadrupole splitting of maximum probability and W_{dis} the distribution half-width.

dip and a lower FWHM than the high-velocity line (Fig. 5). A spectrum taken in an extended velocity range of ± 5 mm/s shows that this asymmetry is not due to the presence of Fe^{2+}. Because of the pronounced asymmetry, the room-temperature spectrum could not be adequately fitted with a single distribution of quadrupole doublets with identical isomer shifts (a model that is appropriate to fit room-temperature spectra of most poorly crystalline iron oxides). Fitting the spectrum with a quadrupole-splitting distribution that implies a linear correlation between the quadrupole splitting and the isomer shifts or the use of two discrete quadrupole-splitting distributions with different isomer shifts, however, leads to acceptable results. Both models indicate a quadrupole splitting of maximum probability for schwertmannite of 0.64 mm/s (Table 4).

The liquid-helium spectrum shows schwertmannite to be magnetically ordered at 4.2 K, but the spectrum is again asymmetric with the first (low velocity) line showing a higher dip and lower FWHM than the sixth line (Fig. 6). The data can not be satisfactorily fitted with a distribution of
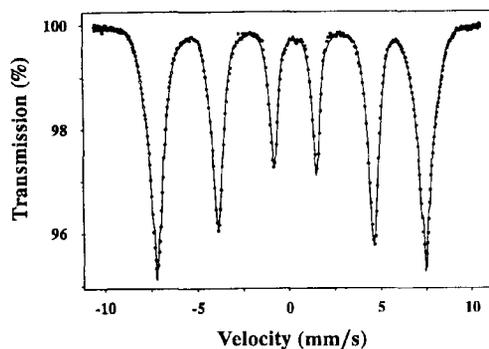

FIG. 6. Mössbauer spectrum of schwertmannite (sample Py-4) recorded at 4.2 K.

magnetic hyperfine fields with identical quadrupole splittings and isomer shifts. Better results are achieved using fits that imply variations of quadrupole splittings as a function of the hyperfine field or two discrete hyperfine field distributions with different isomer shifts and quadrupole splittings. Both models indicate a hyperfine field of maximum probability of 45.6 T (Table 5).

Mössbauer spectra of a synthetic schwertmannite sample (Z500a; cf. Murad, 1988, and Murad *et al.*, 1990) showed the onset of magnetic order to be somewhat smeared out with the relative areas of the magnetic components increasing from 21% at 80 K to 78% at 70 K, indicating an average ordering temperature of 75 K. Spectra taken between 75 and 90 K under an applied magnetic field of 6 T show that a distribution of Néel temperatures and not superparamagnetic relaxation causes the gradual magnetic ordering.

Different locations of iron atoms relative to sulphate groups in schwertmannite could lead to the development of slightly different iron sites. The asymmetry of the Mössbauer spectra both in the paramagnetic and magnetically ordered states and the range of magnetic ordering temperatures indicate that such variability exists. The sulphate could also disrupt magnetic interactions, thus causing the observed low magnetic ordering temperature and magnetic hyperfine field as compared to those of poorly crystalline iron oxides (e.g. ferrihydrite).

Crystal structure

A direct determination of the crystal structure of schwertmannite was not possible because of small crystal size and short-range order. Based on a comparative analysis of synthetic specimens, the mineral is believed to have a hollandite/akaganéite

TABLE 5. Mössbauer parameters of schwertmannite (sample Py-4) at 4.2 K

Fit	B_{max}[‡]	W_{dis}[‡]	δ/Fe	Δ	$\delta(\Delta)$
VAREQ[†]	45.6(1)	3.9	0.492(1)	−0.408(5)	0.022(1)
TWODIS[†]	45.4(1)	3.5	0.493(1)	−0.368(4)	
	45.8(1)	3.5	0.490(1)	−0.082(4)	

[†]VAREQ fits variable quadrupole interactions which increase from the minimum Δ by $\delta(\Delta)$ mm/s per 1.5 T increment in hyperfine field; TWODIS fits two distributions of hyperfine fields with different quadrupole splittings and isomer shifts.

[‡] B_{max} is the hyperfine field of maximum probability and W_{dis} the distribution half-width.

structure type (Bigham *et al.*, 1990). The akaganéite structure consists of double chains of edge-sharing $FeO_3(OH)_3$ octahedra extending along the *c* axis. The octahedra comprising the double chains share corners with adjacent chains to form tunnels approximately 5 × 5 Å in size. In akaganéite, each tunnel is composed of adjoining cavities formed by 8 OH groups. Infrared studies indicate that at least half of these groups are replaced by SO_4^{2-} in schwertmannite to form a bridged bidentate complex of type -Fe-O-SO_2-O-Fe- with Fe atoms on adjacent sides of a cavity. The S and the remaining two 'free' oxygens in the SO_4^{2-} ion must then occupy consecutive cavities parallel to the tunnel axis. Normal bond distances between exposed OH groups on adjacent faces of a cavity are approximately 3.5 Å whereas the O-O distance in the free SO_4^{2-} ion is only about 2.6 Å. Consequently, the structure must be highly distorted in the *a* dimension, which is consistent with the poor crystallinity of the mineral. The proposed distribution of SO_4 also requires that at least two distinctly different Fe sites occur within the structure, one in which Fe sits in its usual octahedral coordination with O and OH as $FeO_3(OH)_3$ and one in which OH is replaced by SO_4 to yield $FeO_3(OH)_2O$-SO_3. The physical existence of multiple Fe sites is readily confirmed by Mössbauer spectroscopy (see previous discussion).

Because the SO_4 fills two adjacent tunnel cavities, a primitive tetragonal cell with *a* = 10.66 and *c* = 6.04 Å is proposed to describe the structure. Experimentally, a doubling of *c* relative to akaganéite is supported by the apparent development of (111) interference with increasing SO_4 content in both natural and synthetic samples (Bigham *et al.*, 1990). A unit cell would then include 16 Fe octahedra surrounding two cavities of a central tunnel. If all tunnel sites are filled, the unit cell formula would be $Fe_{16}O_{16}(OH)_{12}(SO_4)_2$.

Other known occurrences

Samples bearing schwertmannite have been collected from over 40 different locations in Europe, North America and Australia, and data from some of these specimens have been published in earlier reports (Brady *et al.*, 1986; Bigham *et al.*, 1990, 1992; Murad *et al.*, 1990; Fitzpatrick *et al.*, 1992; Fanning *et al.*, 1993). All known occurrences of schwertmannite are related to the surface or near-surface oxidation of metal sulphides. In most instances, sulphide decomposition has been triggered by anthropogenic activities such as mining, road construction, soil drainage, etc; however, a purely natural occurrence of schwertmannite has also been identified in the Zillertaler Alps at approximately 2600 m above sea level. At this location a small, acidic stream originating from a pyritic schist has produced a jarosite-schwertmannite-ferrihydrite paragenetic sequence over an altitudinal distance of approximately 500 m (unpublished data). In general, the widespread distribution of acid sulphate systems should make schwertmannite a mineral of considerable geochemical significance.

The aggregate of samples collected to date have shown a well-defined range in sulphate content. The proposed unit cell formula for schwertmannite is $Fe_{16}O_{16}(OH)_{12}(SO_4)_2$, which corresponds to an Fe/S ratio of 8. Observed Fe/S ratios are usually lower (e.g. see data for sample Py-4 in Table 2) and fall within a range of 4.7 to 8.3. Kinetic data from acid dissolution experiments have shown that lower ratios are due to the adsorption of excess SO_4 on the high surface area particles of schwertmannite (Bigham *et al.*, 1990). Consequently, the combined experimental data support a more general unit cell formula of $Fe_{16}O_{16}(OH)_y(SO_4)_z \cdot nH_2O$, where $16 - y = 2z$ and $2.0 \leqslant z \leqslant 3.5$.

Acknowledgements

References

Bigham, J. M., Schwertmann, U., Carlson, L. and Murad, E. (1990) A poorly crystallized oxyhydroxysulfate of iron formed by bacterial oxidation of Fe(II) in acid mine waters. *Geochim. Cosmochim. Acta*, **54**, 2743–58.

Bigham, J. M., Schwertmann, U. and Carlson, L. (1992) Mineralogy of precipitates formed by the biogeochemical oxidation of Fe(II) in mine drainage. In: *Biomineralization processes of iron and manganese: modern and ancient environments* (H. C. W. Skinner and R. W. Fitzpatrick, eds.), Catena Supplement 21, Catena-Verlag, Cremlingen-Destedt, 219–32.

Brady, K. S., Bigham, J. M., Jaynes, W. F. and Logan, T. J. (1986) Influence of sulfate on Fe-oxide formation: comparisons with a stream receiving acid mine drainage. *Clays Clay Minerals*, **34**, 266–74.

Commission Internationale de l'Eclairage (1978) *Recommendations on uniform colour spaces, colour difference and psychometric colour terms*. Publ. 15, Suppl. 2, Colourimetry. CIE 1971, Paris.

Fanning, D. S., Rabenhorst, M. C. and Bigham, J. M. (1993) Colors of acid sulfate soils. In: *Soil color* (J. M. Bigham and E. J. Ciolkosz, eds.), Soil Sci. Soc. Am. Spec. Pub. 31, p. 91–108.

Fitzpatrick, R. W., Naidu, R. and Self, P. G. (1992) Iron deposits and microorganisms in saline sulfidic soils with altered soil water regimes in South Australia. In: *Biomineralization processes of iron and manganese: modern and ancient environments* (H. C. W. Skinner and R. W. Fitzpatrick, eds.), Catena Supplement 21, Catena-Verlag, Cremlingen-Destedt, 263–86.

Janik, L. M. and Raupach, M. (1977) *An iterative, least-squares program to separate infrared absorption spectra into their component bands*. CSIRO Div. Soils Tech. Paper 35, 1–37.

Lazaroff, N., Sigal, W. and Wasserman, A. (1982) Iron oxidation and precipitation of ferric hydroxysulphates by resting *Thiobacillus ferrooxidans* cells. *Appl. Environ. Microbiol.*, **43**, 924–38.

Lazaroff, N., Melanson, L., Lewis, E., Santoro, N. and Pueschel, C. (1985) Scanning electron microscopy and infrared spectroscopy of iron sediments formed by *Thiobacillus ferrooxidans*. *Geomicrobiol. J.*, **4**, 231–68.

Murad, E. (1988) The Mössbauer spectrum of 'well'-crystallized ferrihydrite. *J. Magnetism Magnetic Mater.*, **74**, 153–7.

Murad, E., Bigham, J. M., Bowen, L. H. and Schwertmann, U. (1990) Magnetic properties of iron oxides produced by bacterial oxidation of Fe^{2+} under acid conditions. *Hyperfine Interactions*, **58**, 2373–6.

[Manuscript received 6 December 1993]